ACS Catalysis

Research Article

pubs.acs.org/acscatalysis

Comparison of Tungsten and Molybdenum Carbide Catalysts for the Hydrodeoxygenation of Oleic Acid

Stefan A. W. Hollak,[†,‡] Robert W. Gosselink,[§,‡] Daan S. van Es,*[,†] and Johannes H. Bitter*[,§,⊥]

[†]Food and Biobased Research, Wageningen University and Research Centre, P. O. Box 17, 6700AA Wageningen, The Netherlands

[§]Inorganic Chemistry and Catalysis, Utrecht University, Universiteitsweg 99, 3584CG Utrecht, The Netherlands

[⊥]Biobased Commodity Chemistry, Wageningen University and Research Centre, P. O. Box 17, Wageningen, 6700AA, The Netherlands

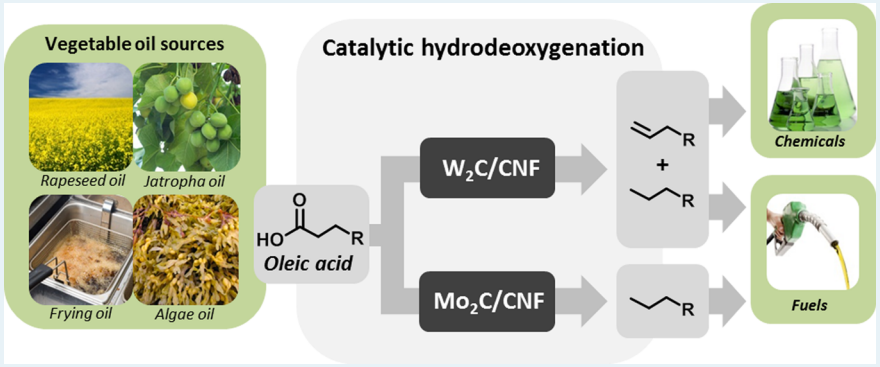

ABSTRACT: Group 6 (W, Mo) metal carbide catalysts are promising alternatives to hydrodesulfurization (NiMo, CoMo) catalysts and group 10 (Pd) type catalysts in the deoxygenation of vegetable fats/oils. Herein, we report a comparison of carbon nanofiber-supported W_2C and Mo_2C catalysts on activity, selectivity, and stability for the hydrodeoxygenation of oleic acid to evaluate the catalytic potential for the upgrading of fat/oil feeds. W_2C/CNF was more selective toward olefins, whereas Mo_2C/CNF was more selective toward paraffins. This was related to the hydrogenation activities of the respective metal carbides. Mo_2C/CNF showed higher activity and stability compared with W_2C/CNF.

KEYWORDS: *hydrodeoxygenation, metal carbides, tungsten, molybdenum, oleic acid*

INTRODUCTION

Fats and oils consist of triglycerides and free fatty acids (FFAs; mainly present in nonedible or waste feedstocks) and are a potential renewable feedstock for transportation fuels since the hydrocarbon chains of these fats and oils are typically in the diesel range. The use of nonedible resources is preferred as feedstock to avoid diverting vegetable fats/oils from food production to biodiesel production; this is generally known as the food vs fuel debate.

Nonedible resources for vegetable oils are algae[1] and jatropha oil[2] and waste fats and oils.[3] The relatively high oxygen content and acidity of this feedstock compared with fossil fuels, however, gives rise to several drawbacks as a fuel, such as corrosive properties and higher viscosity. Deoxygenation (DO) of the vegetable oils is a well-known upgrading process to arrive at hydrocarbons in the diesel range to reduce engine compatibility issues. The hydrocarbons produced via this process could even outperform fossil-based fuels with cetane numbers ranging from 85 to 99, compared with 45−55 for petroleum diesel.[4]

In addition, deoxygenation of vegetable fats and oils is an interesting route to arrive at (higher value) chemicals by tuning selectivity toward the production of olefins or alcohols.[5] Vegetable fats and oils can thus be regarded as promising renewable feedstocks for the production of both fuels and chemicals.

Deoxygenation of triglycerides (in the presence of hydrogen) occurs mainly via β-elimination with subsequent deoxygenation of the intermediate fatty acids, as was comprehensively described in our earlier work.[6] The deoxygenation can occur via three different pathways: decarbonylation, decarboxylation, and hydrodeoxygenation, as shown in Scheme 1. Mainly two classes of catalysts are studied for the DO of vegetable fats/oils and their model compounds: hydrodesulfurization (HDS) catalysts (e.g., sulfided CoMo or NiMo oxides) and group 10 type catalysts.[3,6−12] HDS type catalysts are selective to hydrodeoxygenation (HDO), and group 10 metal catalysts, in particular Pd, are selective to decarbonylation or decarboxylation (DCO).

The main disadvantage of using noble metals such as Pd is their scarcity and, therefore, high costs. HDS type catalysts are less expensive but require activation, that is, a sulfidation

Received: August 29, 2013
Revised: October 16, 2013
Published: October 21, 2013

   dx.doi.org/10.1021/cs400744y | ACS Catal. 2013, 3, 2837−2844

Scheme 1. Pathways for the Deoxygenation (DO) of Fatty Acids

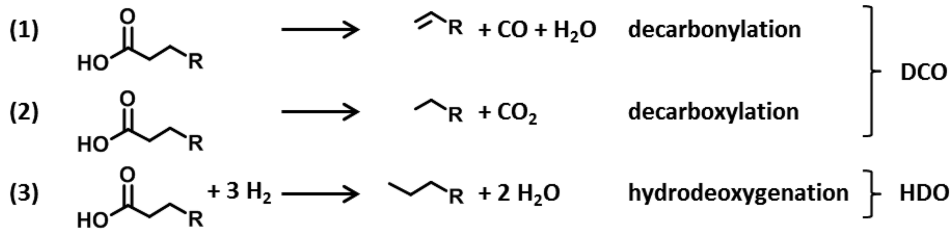

treatment. This might lead to sulfur leaching, which deactivates the catalyst and results in sulfur contamination of the products.[13,14]

Mo_2C-[15] and W_2C-based[16] catalysts have recently been reported as promising materials for deoxygenation catalysts. A direct comparison of the performance of these catalysts is, however, difficult because the experimental data on these studies are not obtained under identical conditions. Moreover, the reports on W_2C-based catalysts describe only the use of saturated feeds. It is, however, necessary to investigate the potential of the W_2C/CNF (CNF = carbon nanofibers) catalyst for unsaturated fatty acids, as well, because these acids comprise the major part of the naturally abundant vegetable fat-/oil-based feeds.

In this work, we report on the application and comparison of molybdenum and tungsten carbide catalysts supported on CNF for the HDO of oleic acid. These catalysts are for the first time compared under the same conditions in deoxygenation activity, selectivity, and stability of unsaturated fatty acids. Furthermore, deoxygenation pathways are suggested by a study of the reactivity of intermediate products observed during the reaction. CNF is used as a support material because of its high specific surface area and mesoporosity. Catalyst characterization is performed by N_2-physisorption, X-ray diffraction (XRD), and X-ray photoelectron spectroscopy (XPS).

EXPERIMENTAL SECTION

Catalyst Synthesis. A 5 wt % Ni/SiO_2 growth catalyst was prepared by homogeneous deposition precipitation as reported earlier[17] using 30 g of SiO_2 (Aerosol 300, Degussa), 7.9 g of $Ni(NO_3)_2$ (Acros Organics), and 4.85 g of urea (Acros Organics) at 90 °C for 18 h in 1.5 L of demineralized water. A 5 g portion of Ni/SiO_2 was subsequently reduced at 700 °C (ramp 5 °C/min in N_2/H_2 flow) in a H_2/N_2 flow for 2 h. Fishbone type CNFs were obtained by flowing a $CO/H_2/N_2$ mixture (266/102/450 mL/min) at an overpressure of 3 bar over this catalyst at 550 °C (ramp 5 °C/min in N_2/H_2 flow) for 24 h.

The crude product, ~35 g, was collected and refluxed three times for 1 h in 0.4 L of boiling 1.0 M KOH (Acros) to remove SiO_2. The product was washed with deionized water between the refluxing cycles. Subsequently, the fibers were treated with 0.4 L of boiling, concentrated HNO_3 (65%, Merck) for 1.5 h to remove exposed nickel and introduce oxygen-containing groups. It should be noted that some Ni can still be present after the HNO_3 treatment, as has been reported earlier.[18] This is encapsulated Ni and cannot be removed by a HNO_3 treatment, but as such, it is unlikely to play a role in catalysis. The acid-treated fibers were finally washed with demineralized water until the pH of the filtrate was neutral.

The CNF were dried under vacuum at 80 °C for 4 h prior to impregnation. For the tungsten-based catalysts, the support was impregnated using ammonium metatungstate (66.5 wt % W, Aldrich) by pore volume impregnation (0.7 mL/g, determined by water uptake) to arrive at a 15 wt % W loading. After impregnation, the sample was kept under vacuum at 80 °C for 24 h. A heat treatment was subsequently applied for 3 h at 1000 °C (5 °C/min) under N_2 flow to yield W_2C/CNF. Mo_2C/CNF was also prepared by pore volume impregnation using an ammonium molybdate (>99%, Acros) solution to arrive at a 7.5 wt % Mo loading, followed by a heat treatment at 900 °C for 3 h under N_2 flow.

Catalyst Characterization. N_2-physisorption isotherms were recorded with a Micromeritics Tristar 3000 at 77 K. Prior to performing the measurement, the samples were dried for at least 16 h at 473 K in an N_2 flow. The surface area was determined using the Brunauer–Emmett–Teller (BET) theory.[19] The total pore volume was defined as the single-point pore volume at $p/p_0 = 0.95$.

XRD patterns were obtained with a Bruker-AXS D2 Phaser powder X-ray diffractometer using Co $K\alpha_{1,2}$ with $\lambda = 1.79026$ Å, operated at 30 kV, 10 mA. Measurements were carried out between 10° and 100° 2θ using a step size of 0.09° 2θ and a scan speed of 1 s/step.

Imaging of the sample was done through transmission electron microscopy (TEM), performed using an FEI TECNAI20F transmission electron microscope operated at 200 keV. The instrument is equipped with a Schottky field emission gun and a twin objective lens. The magnification range is 25–700 k*x*, the point-to-point resolution was 0.27 nm, and the lattice image resolution was 0.14 nm. The images were made with a Megaview II digital camera. The samples were suspended in ethanol using an ultrasonic treatment and brought onto a holey carbon film on a copper grid.

X-ray photoelectron spectroscopy (XPS) characterization was performed using a JPS-9200 photoelectron spectrometer (JEOL, Japan). Spectra were collected using Al Kα X-ray radiation at 10 kV and 20 mA with an analyzer pass energy of 50 eV for wide scans and 10 eV for narrow scans. Analysis of XPS data was performed using CasaXPS software (Casa Software Ltd., Teignmouth, UK).

Catalytic Testing. Catalytic experiments were carried out in a 100 mL EZE Autoclave Engineer Batch reactor. The reactor was loaded with 0.25 g of catalyst, 2.00 g of oleic acid (Aldrich, 90%, also contains stearic acid and linoleic acid), 1.00 g of tetradecane (internal standard, Aldrich, 99%), and 50 mL of dodecane (Acros, 99.9%) as solvent. Subsequently, the reactor was pressurized with hydrogen (50 bar at reaction temperature) and heated to 350 °C (5 °C/min). The reaction mixture was stirred with an overhead mechanical stirrer during

dx.doi.org/10.1021/cs400744y | ACS Catal. 2013, 3, 2837–2844

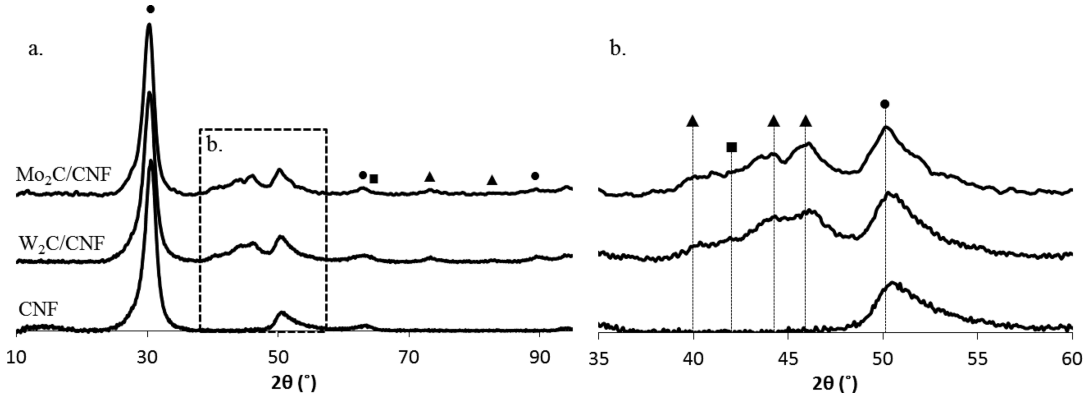

Figure 1. XRD diffractogram overview and zoom of CNF, W_2C/CNF, and Mo_2C/CNF. Diffraction lines are given for graphitic carbon (●), XO_x (■), and X_2C (▲), with X = W, Mo.

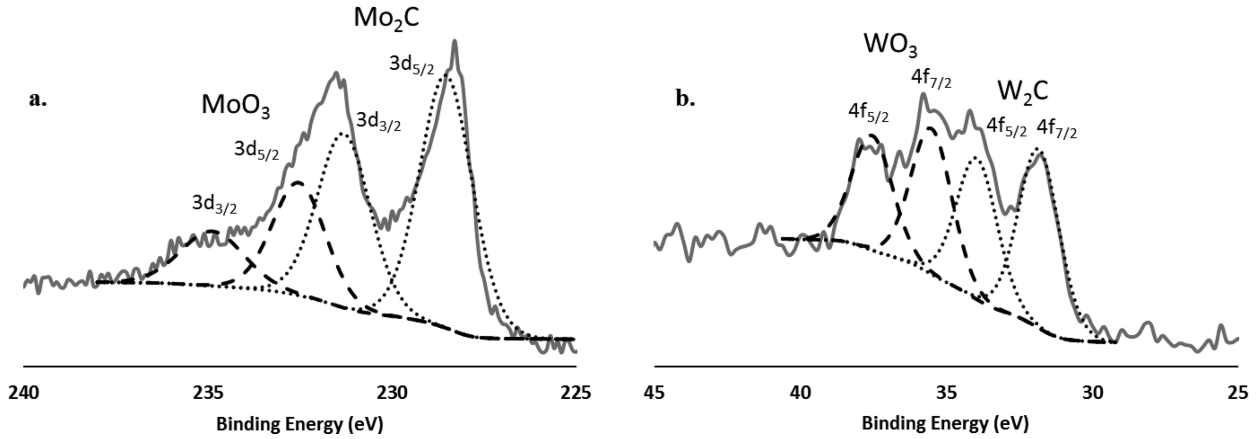

Figure 2. XPS spectra of (a) Mo_2C/CNF and (b) W_2C/CNF, stored in argon. Dashed lines are used for the oxide peaks, and round dots, for the carbide peaks.

the reaction: 600 rpm during heating and 1000 rpm during reaction. Sampling was performed during the catalytic experiments via a preheated dip tube. The sampling procedure did not affect the catalysis, confirmed by comparing a catalytic experiment with and without intermediate sampling, which resulted in comparable catalyst activity and product selectivity. The reactor was quenched with an ice−water bath after the desired reaction time.

Product Analysis. Reaction mixture work-up after reaction and cooling was performed with a $CHCl_3$/MeOH (2:1) mixture that was heated to 40 °C to ensure complete dissolution of the fatty acid. A sample was subsequently taken from the mixture and methylated by mixing with trimethylsulfonium hydroxide (TMSH, purum, ≈0.25 M in methanol, Aldrich), an in situ esterification reagent to derivatize carboxylic acids for accurate GLC quantification.

Analysis of low-molecular-weight (up to ∼350 g mol^{-1}) products was performed on a Theromo Focus gas chromatograph (GC) equipped with an automatic injection system (AS3000 autosampler). The following parameters/settings were used: injection volume, 1 μL; split ratio, 1:20; column pressure, 150 kPa helium; GC column, Varian CP-FFAP (free fatty acids), 25 m × 0.32 mm × 0.30 μm; detector, FID at 280 °C; injection port temperature, 250 °C. GC program: hold 1 min at 50 °C, ramp 7 °C/min to 150 °C, ramp 4 °C/min to 250 °C, and hold at 250 °C for 20 min.

Analysis of fatty acid esters and other relatively large molecules was performed on a Hewlett-Packard 5890 Series II gas chromatograph equipped with an automatic injection system (HP7673 GC/SFC injector and controller). Injection volume, 1 μL; split ratio, 1:20; column pressure, 150 kPa Helium; GC column, Varian Select Biodiesel for Glycerides, 15 m × 0.32 mm × 0.45 μm; detector, FID at 280 °C; injection port temperature, 380 °C. GC program: hold 1 min at 50 °C, ramp 7 °C/min to 150 °C, ramp 4 °C/min to 240 °C, ramp 9 °C/min to 380 °C, and hold 1 min at 380 °C.

GC/MS analyses were performed on an Interscience TraceGC Ultra GC with AS3000 II autosampler. He carrier gas; flow 1 mL/min; split flow, 20 mL/min; Restek GC column Rxi-5 ms, 30 m × 0.25 mm × 0.25 μm. GC program: hold 1 min at 50 °C, ramp 7 °C/min to 150 °C, ramp 4 °C/min to 340 °C, and hold at 340 °C for 20 min. The GC column is connected to an Interscience TraceDSQ II XL quadrupole mass-selective detector (EI, mass range 35−500 Da, 150 ms sample speed).

RESULTS

Catalyst Characterization. XRD analysis was performed to analyze the catalyst phases. The diffractograms of the fresh W_2C/CNF and Mo_2C/CNF catalysts after impregnation and heat treatment and bare CNF are shown in Figure 1. Bare CNF shows typical diffraction lines at 31° and 51° 2θ representing graphite like carbon. The introduction of Mo_2C and W_2C onto the CNF results in peaks at 40, 44, and 46° 2θ, which correspond to the (110), (002), and (111) carbide-phase

dx.doi.org/10.1021/cs400744y | ACS Catal. 2013, 3, 2837−2844

diffraction lines.[20] These occur at identical angles for Mo_2C and W_2C because of their identical crystal structures and ionic radii. The diffraction peak at 43° 2θ indicates the presence of an oxide phase, either WO_x or MoO_x ($2 < x < 3$). The existence of these phases can be explained by either incomplete carburization of the catalysts or partial oxidation of the carbide phase due to exposure to air when the sample is transferred to the XRD equipment.

Next to XRD, which is a bulk characterization technique, X-ray photoelectron spectroscopy (XPS) is used for catalyst characterization. Figure 2 shows the XPS spectra of the Mo_2C/CNF and W_2C/CNF catalysts, which were stored under argon after their preparation. Short contact time with air, however, could not be excluded when preparing the samples for XPS. Both samples display carbide peaks: at 228 and 231 eV for Mo_2C/CNF (Figure 2a) and at 32 and 34 eV for W_2C/CNF (Figure 2b).[21] The existence of the carbide phase is thus also confirmed at the (sub)surface of both catalysts.

For Mo_2C/CNF, the peaks at 232 and 235 eV can be attributed to MoO_3 (Figure 2a), whereas WO_3 peaks are visible at 35 and 37 eV for the W_2C/CNF sample (Figure 2b). The appearance of these oxides can be explained by partial oxidation of the carbide surface by contact with air. A comparison of the oxide peak areas relative to the carbide peaks shows a higher content of oxide species relative to the carbide contribution for the tungsten-based catalyst. It should be noted that the different metal carbide catalysts can be (qualitatively) compared only at similar dispersions (which is the case here; see Table 1) and at a similar inelastic mean free path (imfp) of the photoelectron via XPS. Calculations of the latter using the QUASES-IMFP-TPP2M program reveal a difference in imfp between tungsten- and molybdenum-based catalysts of ~10%. This cannot, however, explain the differences in oxide content of the metal carbide catalysts in Figure 2 because these are much larger than 10%. The differences in oxide content could indicate that the tungsten-based catalyst is more prone to oxidation. Alternatively, the higher oxide content for the tungsten-based catalyst can also be related to incomplete carburization.

Table 1. Physicochemical Characteristics of the CNF-Supported Metal Carbide Catalysts under Study

	particle size (nm)		N_2 physisorption	
	TEM	XRD	BET surface area (m^2/g)	Pore volume (cm^3/g)
CNF			190	0.40
Mo_2C/CNF	5	4	120	0.34
W_2C/CNF	5	4	111	0.30

The oxide peaks increase when the catalysts are exposed to air for 24 h before XPS analysis (Figure 3), showing that oxidation does occur for both catalysts. However, carbide peaks are still present. W_2C/CNF again shows a higher oxide content relative to the carbide phase as compared with Mo_2C/CNF, confirming that this catalyst is more sensitive to oxidation.

The samples that were exposed to air for 24 h were also characterized by XRD (not shown). For both catalysts, similar diffractograms were obtained, as compared with the fresh catalysts (Figure 1). This illustrates that the bulk of the materials is still in their carbidic form. It can thus be concluded that mainly (sub)surface oxidation occurs, albeit to a larger extent for tungsten carbide.

Further physicochemical characterization of the carbide catalysts was performed with XRD and TEM to determine the metal particle size (Table 1). The metal particle size was calculated via XRD using the Scherrer equation and particle size histograms from TEM images.[22] These calculations resulted in an average particle size of 4−5 nm for both catalysts (Table 1). As such, qualitative comparison between both metal carbide catalysts can be made.

N_2 physisorption was also performed on the bare support material and the two metal carbide catalysts to compare the BET surface area and pore volume. As shown in Table 1, both the BET surface area and the pore volume decrease as a result of impregnation because the metal carbide particles occupy part of the carbon surface. In addition, some pore blocking could also have occurred during impregnation.

Catalytic Tests. The catalytic experiments were performed at 350 °C under 50 bar H_2 pressure. Identical reaction conditions were used for both catalysts for comparison, and the reaction temperature of 350 °C was chosen because W_2C/CNF was reported to be active at this reaction temperature.[16] For a comparison of the two carbide catalysts, it is also important to exclude possible effects of pressure-differences due to gas consumption during catalytic experiments. For this reason, a 50 bar H_2 was used during the catalytic experiments.

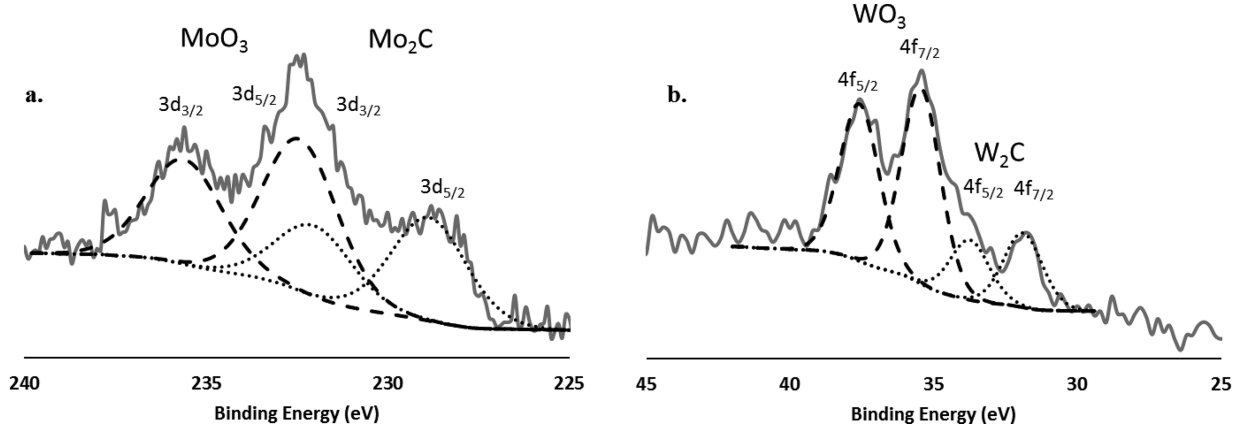

Figure 3. XPS spectra of (a) Mo_2C/CNF and (b) W_2C/CNF, exposed to air for 24 h. Dashed lines are used for the oxide peaks, and round dots, for the carbide peaks.

dx.doi.org/10.1021/cs400744y | ACS Catal. 2013, 3, 2837−2844

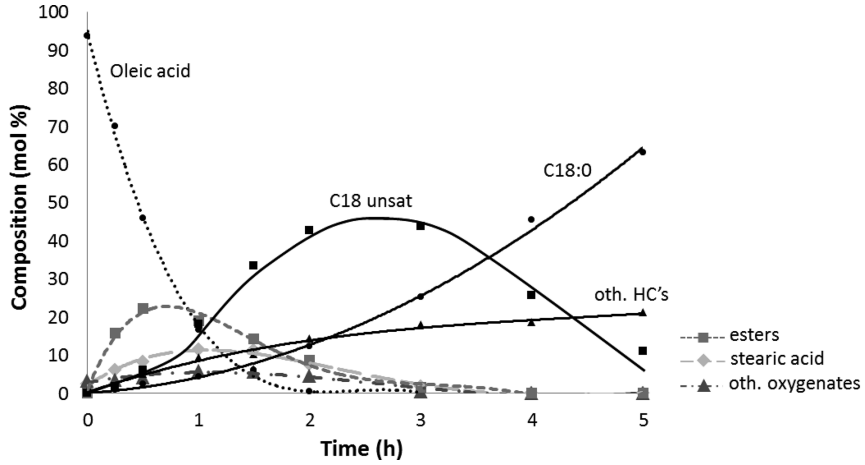

Figure 4. Composition of reaction mixture over time for W_2C/CNF. Reaction conditions: T = 350 °C, p = 50 bar H_2, t = 5 h, $m_{oleic\ acid}$ = 2 g, m_{cat} = 0.25 g, $m_{dodecane}$ = 36 g.

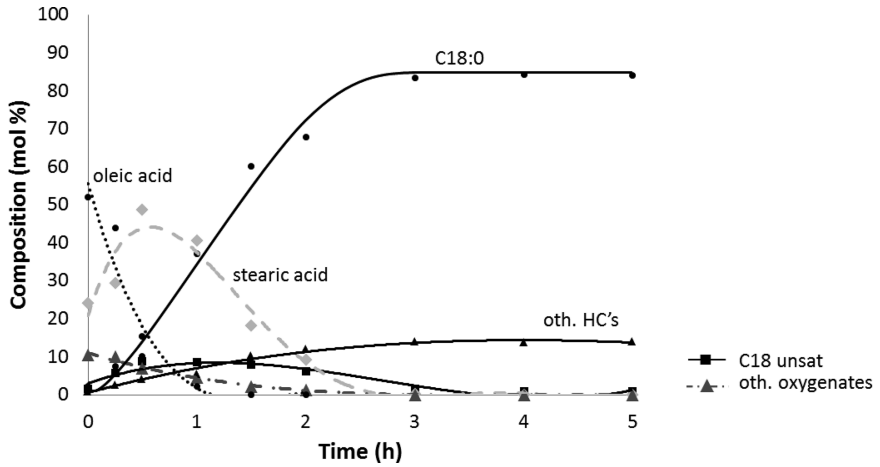

Figure 5. Composition of reaction mixture over time for Mo_2C/CNF. Reaction conditions: T = 350 °C, p = 50 bar H_2, t = 5 h, $m_{oleic\ acid}$ = 2 g, m_{cat} = 0.25 g, $m_{dodecane}$ = 36 g.

Figure 4 shows the product yields for the W_2C/CNF catalyst as a function of time using oleic acid as the feed. Full conversion of oleic acid was attained within 2 h. Stearic acid and other oxygenates (other HC's) were already present in the reaction mixture at t = 0 (when the reaction mixture reached 350 °C). Octadecenol isomers were observed with varying positions of the C═C double bond, indicating that isomerization of the C═C double bond occurs under the applied conditions. Octadecanal, octadecenol, and octadecanol are known intermediates for the hydrodeoxygenation of fatty acids.[6,14,16,23] Esters (formed by esterification of fatty acid with fatty acid alcohol) were present after a short inhibition period, as expected for a secondary product. The intermediate character of the different oxygenates is also shown in Figure 4 by the initial increase, followed by a decrease at higher oleic acid conversion. The decrease in esters can be attributed to the esterification equilibrium, which shifts toward hydrolysis upon the deoxygenation of C18 alcohols to yield octadecene/octadecane and water.

The formation of unsaturated C18 hydrocarbons (C18 unsat) increased during the first 2 h of the reaction, after which it decreased as a result of hydrogenation to octadecane (C18:0), of which the amount increased up to 60 mol % after 5 h of reaction time. The molar balance is stable over time (between 85 and 90%), indicating the absence of heavy product formation and cracking reactions over time. The loss in mass balance could be due to adsorption of feeds or products on the catalyst surface; for instance, via the cis C−C double bond of unsaturations.[24] Furthermore, catalyst coking could also occur, especially because unsaturations are reported to be prone to coke reactions.[6,25−27] However, the sampling and workup procedure could also affect the mass balance slightly.

Figure 5 shows that full conversion of oleic acid was already attained at t = 0.75 h over Mo_2C/CNF. In addition, at t = 0, only 50 mol % of the initial amount of oleic acid was left. The high conversion at t = 0 indicates that conversion of oleic acid already occurred during the heat up (heat up time 0.3 h from 250 °C, no activity below 250 °C). Simultaneously, the formation of mainly stearic acid and alcohols also occurred during the heating stage, which subsequently decreased again at high conversion levels. Negligible ester formation was observed, whereas the yield of other oxygenates (consisting of mainly alcohols) was already 10 mol % at t = 0. It should be noted that the content of intermediate oxygenates was significantly lower as compared with the reaction over W_2C/CNF. The unsaturated C18 content decreased rapidly, followed by the formation of octadecane, which showed a stable product yield around 80 mol % after t = 3 h.

dx.doi.org/10.1021/cs400744y | ACS Catal. 2013, 3, 2837−2844

Scheme 2. Fatty Acid Conversion Pathways, With Observed Intermediates, Catalysed by Tungsten and Molybdenum Carbide

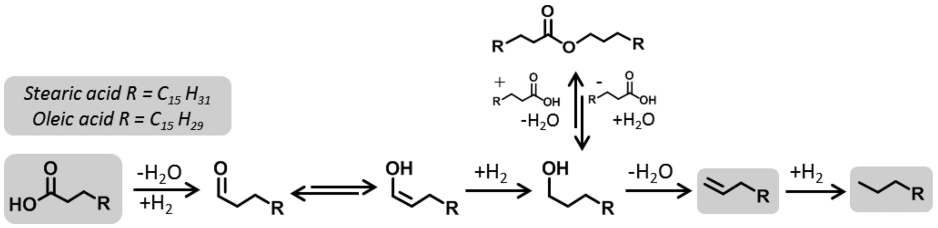

Thus, on the basis of the relatively fast hydrogenation of oleic acid to stearic acid combined with the low olefinic product content, it must be concluded that Mo_2C/CNF is a more active hydrogenation catalyst than W_2C/CNF. In addition, Figures 4 and 5 show that the initial formation of hydrocarbon products, that is, both saturated and unsaturated, was higher for Mo_2C/CNF than for W_2C/CNF. The initial formation of stearic acid (up to 50 mol %) over Mo_2C/CNF indicates that the double bond of oleic acid was hydrogenated before deoxygenation occurred. This confirms the higher hydrogenating activity of Mo_2C. It should be noted that direct DO of oleic acid to hydrocarbons, which has been proposed before, cannot be excluded.[6]

After the formation of stearic acid by hydrogenation, it has been claimed that the next step is the formation of an aldehyde that is in equilibrium with its enol form (see Scheme 2).[16,23] This explains the observed formation of aldehydes and alcohols. The unsaturated C18 alcohol can then be further hydrogenated to a saturated alcohol; dehydrated to an alkene; and finally, hydrogenated to a saturated hydrocarbon (Scheme 2). For W_2C/CNF, it has already been shown that the reaction yields mainly the unsaturated hydrocarbon.[15,16] Significantly lower amounts of unsaturated hydrocarbons and oxygenates were observed for the Mo_2C/CNF-catalyzed deoxygenation of oleic acid, confirming its higher hydrogenation properties as compared with W_2C/CNF.

Higher molar balances (95−100%) were obtained for Mo_2C/CNF compared with W_2C/CNF (85−90%). In addition, here, the molar balance remained stable during the experiment. The difference in molar balance is suggested to be related to the fast hydrogenation of unsaturations over Mo_2C/CNF, resulting in a decreased concentration of reactive compounds, which are known to be coke precursors.[28,29] Comparable observations were made by Berenblyum et al. for the decarbonylation of stearic acid over Pd, Pt, Ni, and Cu supported on Al_2O_3.[30] For Cu, a high selectivity to undesired side reactions was obtained, whereas this was not the case for the other (hydrogenation) catalysts, which showed higher heptadecane selectivities.

It should be noted that both catalysts also showed the formation of other hydrocarbon products (other HC's), which mainly consists of DCO products, that is, heptadecane and heptadecenes. This can be attributed to the presence of surface WO_x species in the case of W_2C/CNF, as has been reported previously.[16] Similar catalytic behavior of the oxide can be expected for the molybdenum-based catalyst. Mo_2C/CNF showed lower C17 product formation compared with W_2C/CNF (7 mol % vs 15 mol %), thereby confirming the higher stability toward oxidation of this carbide, which was also suggested by XPS results (Figures 2 and 3). Regarding the DCO products, it was observed that Mo_2C/CNF showed the formation of only heptadecane, whereas a parallel evolution of heptadecane and heptadecene was obtained for W_2C/CNF, confirming again the higher hydrogenation activity of the former.

A comparison of the catalytic activities and selectivities of the metal carbide catalysts with the already studied metal sulfide and group 10 catalysts is difficult because of the different reaction conditions applied. However, the high DO selectivities, at full conversion, obtained with W_2C/CNF (89 mol %) and Mo_2C/CNF (90 mol %) are comparable to group 10 metal catalysts for the DO of stearic acid, Pd/C (91 mol %),[12] Ni/C (81 mol %),[12] Ni/H-β (98 mol %),[31] and Ni−ZrO_2 (92 mol %).[10] In addition, the average productivity (calculated at 90 mol % conversion of fatty acids) is an order of magnitude higher for the metal carbides, that is, on the order of 10^{-3} compared with 10^{-4} mol DO product × mol metal^{-1} s^{-1}. It should be noted that these experiments, with Pd and Ni catalysts, were performed at lower temperatures (260−300 °C), which strongly affects the catalytic activity. However, these results indicate that these metal carbide catalysts show promising activities and productivities for the DO of fatty acid feeds at the operated reaction conditions.

Catalyst Reuse. Except for catalyst activity and selectivity, catalyst stability was also investigated in comparing the carbide catalysts. Catalyst stability was studied by two methods: washing and washing/recarburization. First, a catalytic test at 350 °C for 1 h and 50 bar H_2 was performed using oleic acid as reactant (run 1). The spent catalyst was then rinsed at ambient conditions with $CHCl_3$/MeOH (2:1) and reused in a catalytic test (run 2). Thereafter, the spent catalyst of run 2 was rinsed at ambient conditions with $CHCl_3$/MeOH (2:1), recarburized as described in the Experimental Section, and again reused for the deoxygenation of oleic acid (run 3). From XRD line-broadening measurements between the runs, particle sizes and catalyst phases were established. The stability runs were performed using only 0.1 g of catalyst (instead of the 0.25 g of catalyst used in earlier experiments) and a reaction time of 1 h to ensure incomplete oleic acid conversion. This was done because catalyst stability cannot be examined at full conversion because a catalyst can deactivate but still show 100% conversion after a second run.

The catalytic data of the W_2C/CNF recycle and regeneration tests are compiled in Table 2. It is shown that the conversion drops from 70 to 48 mol % after 1 run, suggesting significant deactivation. The regeneration treatment resulted in an increase in both the oleic acid conversion and selectivity to intermediates and hydrocarbon products (run 3); however, the obtained conversion of 52 mol % and hydrocarbon selectivity of 15% were still lower compared with those over the fresh catalyst of 70 mol % conversion and 26% hydrocarbon selectivity. The mass balance was similar for the three runs, indicating that the occurrence of unwanted side reactions did not increase for reactions with the reused and recarburized catalyst.

dx.doi.org/10.1021/cs400744y | ACS Catal. 2013, 3, 2837−2844

Table 2. Recycle and Regeneration of W_2C/CNF and Mo_2C/CNF[a]

	W_2C/CNF			Mo_2C/CNF		
	run 1	run 2	run 3	run 1	run 2	run 3
conversion (mol %)	70	48	52	82	73	67
intermediates selectivity (%)[b]	74	88	85	87	93	93
hydrocarbon selectivity (%)	26	12	15	13	7	7

[a]Reaction conditions: T = 350 °C, p = 50 bar H_2, t = 1 h, $m_{oleic\ acid}$ = 2 g, m_{cat} = 0.1 g, $m_{dodecane}$ = 36 g. [b]Selectivity to stearic acid, esters, alcohols, and other oxygenates.

Note that in these studies, relatively low DO selectivities (<30%) and high selectivities to intermediate products (>70%) were obtained as a result of the low catalyst amount and reaction time used.

The fresh tungsten-based catalyst shows typical diffraction peaks for the W_2C phase at 40, 44, and 46° 2θ (Figure 6). A clear increase in the peak at 43° 2θ is visible after run 1, corresponding to the formation of a WO_x phase. A subsequent test on the spent catalyst (run 2) shows a further increase in the intensity of this peak. In addition, the peak becomes sharper, as well, which is indicative of bigger particles. It can thus be concluded that oxidation and subsequent sintering of the carbide phase occurs under the present reaction conditions. A carbide phase, however, is still present after the runs, as well.

Figure 6 shows the formation of an oxide phase and sintering of these oxide particles during the reaction. Previous research on the reusability of W_2C/CNF for the DO of stearic acid also showed the formation of oxide particles during the reaction but did not result in significant deactivation of the catalyst.[16] This indicates that the formation of an oxide phase could not be the main reason for the catalyst deactivation. Instead, the unsaturated feed (as well as the increased amount of unsaturations in the product mixture) mainly contributes to catalyst deactivation, most likely by the formation of coke deposits, which has been proposed to be an issue when using unsaturated feeds under the applied conditions.[32]

A subsequent heat treatment at 1000 °C of the catalyst after run 2 was shown to be effective to carburize the oxide species and obtain mainly W_2C/CNF (Figure 6). The average particle size during this treatment also increased to ∼8 nm. This explains the lower conversion and DO selectivity of run 3 (Table 2). This third catalytic test subsequently again resulted in the increase of the peak at 43° 2θ, indicative of a WO_x contribution.

Similar recycle tests were also performed for Mo_2C/CNF. The catalytic data for the different runs over the molybdenum-based catalyst are presented in Table 2. A decrease in conversion level from 82 to 73 mol % was observed going from run 1 to run 2. Simultaneously, a decrease in the DO selectivity was observed. Nevertheless, the decrease in activity is significantly less pronounced for Mo_2C/CNF as compared with W_2C/CNF.

XRD diffraction patterns of the fresh, spent, and regenerated catalyst show no significant changes for different catalytic tests and a regeneration treatment (diffractogram comparable to Mo_2C/CNF in Figure 1); however, deactivation also occurred for Mo_2C/CNF, although no difference in the catalyst phase was observed by XRD. In addition, here, the unsaturated feed and products are suggested to cause the reported deactivation. This also explains the less pronounced decrease in activity for Mo_2C/CNF compared with W_2C/CNF because the former showed significantly faster hydrogenation of unsaturations in the course of the reaction (Figure 4 and 5).

Comparing Mo_2C/CNF and W_2C/CNF, it can be concluded that the carbide phase in the tungsten-based catalyst is more prone to oxidation and sintering compared with the Mo_2C phase. Deactivation is also shown to be more severe for W_2C/CNF, which is attributed to the lower hydrogenation rate of this catalyst.

As mentioned before, the recycle experiments were performed at low DO selectivity and relatively high concentrations of oxygenated intermediates. For that reason, similar recycle tests were performed at 100 mol % conversion for both catalysts (0.25 g of catalyst, 5 h reaction time) to investigate if the composition of the reaction mixture affects the catalyst phase and particle size. These recycle tests resulted in similar XRD patterns, confirming that the reported effects on the catalyst phase and particle size upon catalyst recycling are independent of the conversion level.

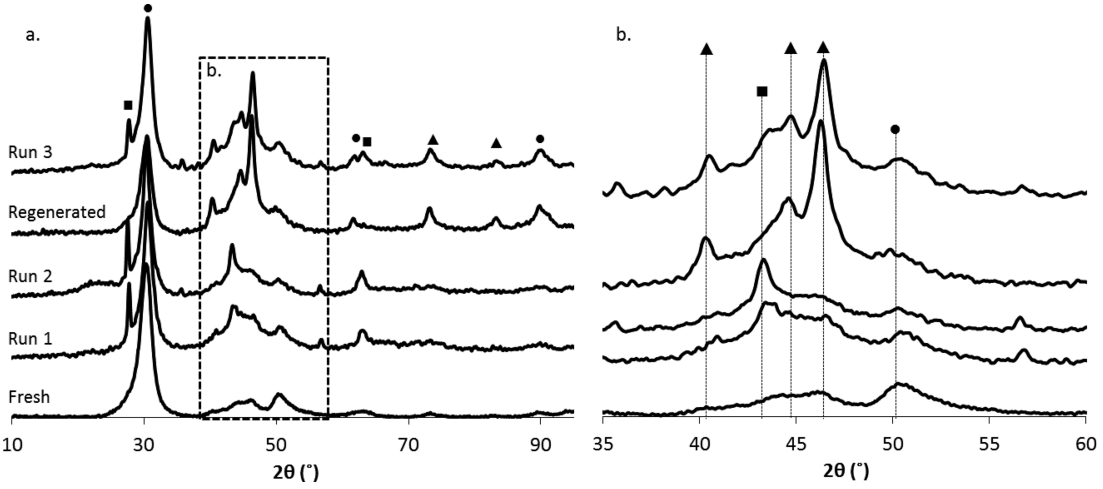

Figure 6. XRD diffractogram of W_2C/CNF upon different recycle tests. Diffraction lines are given for graphitic carbon (●), WO_x (■), and W_2C (▲).

dx.doi.org/10.1021/cs400744y | ACS Catal. 2013, 3, 2837−2844

CONCLUSION

Metal carbide catalysts show promising catalytic properties for the hydrodeoxygenation of unsaturated fatty acids with high selectivities to paraffins or olefins, which are of particular interest for the production of either fuels or chemicals from vegetable fats/oils.

A study on the hydrodeoxygenation of oleic acid over W_2C/CNF and Mo_2C/CNF showed a difference in catalytic behavior between the two carbide catalysts, which was related to the differences in hydrogenation activity. Catalytic experiments over W_2C/CNF showed more olefinic products compared with Mo_2C/CNF, which resulted in a higher deactivation rate of the tungsten based catalyst. This is attributed to the higher hydrogenation rate over Mo_2C/CNF, resulting in less olefins and, thus, in a lower concentration of coke precursors. In addition, W_2C/CNF appeared more sensitive to oxidation compared with Mo_2C/CNF.

W_2C/CNF is shown to be more suitable for the production of high-value olefinic products. Mo_2C/CNF, on the other hand, shows increased activity and catalyst stability in comparison with W_2C/CNF. A trade-off between activity and selectivity has thus to be made regarding the production of olefinic products. Mo_2C/CNF is the preferred catalyst when paraffins for fuels are desired.

AUTHOR INFORMATION

Corresponding Authors

*E-mail: daan.vanes@wur.nl.

*E-mail: harry.bitter@wur.nl.

Author Contributions

‡S.A.W.H. and R.W.G. contributed equally to this paper.

Notes

The authors declare no competing financial interest.

ACKNOWLEDGMENTS

This research has been performed within the framework of the CatchBio program. The authors gratefully acknowledge the support of the Smart Mix Program of The Netherlands Ministry of Economic Affairs and The Netherlands Ministry of Education, Culture and Science. The authors also express their gratitude to Prof. Dr. ir. Krijn de Jong (UU) and Daniel Stellwagen M.Sc. (UU) for discussions and suggestions. Marcel Giesbers (WUR) is kindly acknowledged for his help with the XPS measurements, and Wouter Teunissen (WUR), for his help with GC and GC/MS.

REFERENCES

(1) Demirbas, A.; Fatih Demirbas, M. *Energy Convers. Manage.* **2011**, *52*, 163−170.

(2) Achten, W. M. J.; Verchot, L.; Franken, Y. J.; Mathijs, E.; Singh, V. P.; Aerts, R.; Muys, B. *Biomass Bioenergy* **2008**, *32*, 1063−1084.

(3) Madsen, A. T.; Ahmed, E. H.; Christensen, C. H.; Fehrmann, R.; Riisager, A. *Fuel* **2011**, *90*, 3433−3438.

(4) Snåre, M.; Mäki-Arvela, P.; Simakova, I. L.; Myllyoja, J.; Murzin, D. Y. *Russ. J. Phys. Chem. B* **2009**, *3*, 1035−1043.

(5) van der Klis, F.; Le Nôtre, J.; Blaauw, R.; van Haveren, J.; van Es, D. S. *Eur. J. Lipid Sci. Technol.* **2012**, *114*, 911−918.

(6) Gosselink, R. W.; Hollak, S. A. W.; Chang, S.-W.; van Haveren, J.; de Jong, K. P; Bitter, J. H; van Es, D. S *ChemSusChem* **2013**, *6*, 1576−1594.

(7) Kubičková, I.; Kubička, D. *Waste Biomass Valorization* **2010**, *1*, 293−308.

(8) Boda, L.; Onyestyák, G.; Solt, H.; Lónyi, F.; Valyon, J.; Thernesz, A. *Appl. Catal., A* **2010**, *374*, 158−169.

(9) Kubička, D.; Kaluža, L. *Appl. Catal., A* **2010**, *372*, 199−208.

(10) Peng, B.; Yuan, X.; Zhao, C.; Lercher, J. A. *J. Am. Chem. Soc.* **2012**, *134*, 9400−9405.

(11) Tiwari, R.; Rana, B. S.; Kumar, R.; Verma, D.; Kumar, R.; Joshi, R. K.; Garg, M. O.; Sinha, A. K. *Catal. Commun.* **2011**, *12*, 559−562.

(12) Santillan-Jimenez, E.; Morgan, T.; Lacny, J.; Mohapatra, S.; Crocker, M. *Fuel* **2012**, *103*, 1010−1017.

(13) Kubička, D.; Horáček, J. *Appl. Catal., A* **2011**, *394*, 9−17.

(14) Senol, O. I.; Ryymin, E.; Viljava, T.; Krause, A. *J. Mol. Cat. A: Chem.* **2007**, *268*, 1−8.

(15) Han, J.; Duan, J.; Chen, P.; Lou, H.; Zheng, X. *Adv. Synth. Catal.* **2011**, *353*, 2577−2583.

(16) Gosselink, R. W.; Stellwagen, D. R.; Bitter, J. H. *Angew. Chem.* **2013**, *125*, 5193−5196.

(17) Toebes, M. L.; van der Lee, M. K.; Tang, L. M.; Huis in 't Veld, M. H.; Bitter, J. H.; van Dillen, A. J.; de Jong, K. P. *J. Phys. Chem. B* **2004**, *108*, 11611−11619.

(18) Toebes, M. L.; Prinsloo, F. F.; Bitter, J. H.; van Dillen, A. J.; de Jong, K. P. *J. Catal.* **2003**, *214*, 78−87.

(19) Brunauer, S.; Emmett, P. H.; Teller, E. *J. Am. Chem. Soc.* **1938**, *60*, 309−319.

(20) ICDD PDF-2 database package http://icdd.com/products/pdf2.htm.

(21) Wagner, C. D.; Muilenberg, G. E. *Handbook of X-ray Photoelectron Spectroscopy: A Reference Book of Standard Data for Use in X-ray Photoelectron Spectroscopy*; Physical Electronics Division, Perkin-Elmer Corp.: Eden Prairie, MN, 1979.

(22) Patterson, A. *Phys. Rev.* **1939**, *56*, 978.

(23) Donnis, B.; Egeberg, R.; Blom, P.; Knudsen, K. *Top. Catal.* **2009**, *52*, 229−240.

(24) Immer, J. G.; Kelly, M. J.; Lamb, H. H. *Appl. Catal., A* **2010**, *375*, 134−139.

(25) Snare, M.; Kubickova, I.; Maki-Arvela, P.; Eranen, K.; Murzin, D. Y. *Ind. Eng. Chem. Res.* **2006**, *45*, 5708−5715.

(26) Lestari, S.; Mäki-Arvela, P.; Bernas, H.; Simakova, O.; Sjöholm, R.; Beltramini, J.; Lu, G. Q. M.; Myllyoja, J.; Simakova, I.; Murzin, D. Y. *Energy Fuels* **2009**, *23*, 3842−3845.

(27) Madsen, A. T.; Rozmysłowicz, B.; Simakova, I. L.; Kilpiö, T.; Leino, A.-R.; Kordás, K.; Eränen, K.; Mäki-Arvela, P.; Murzin, D. Y. *Ind. Eng. Chem. Res.* **2011**, *50*, 11049−11058.

(28) Haag, W. O.; Lago, R. M.; Weisz, P. B. *Faraday Discuss. Chem. Soc.* **1981**, *72*, 317−330.

(29) Corma, A.; Orchillés, A. V. *Microporous Mesoporous Mater.* **2000**, *35−36*, 21−30.

(30) Berenblyum, A. S.; Shamsiev, R. S.; Podoplelova, T. A.; Danyushevsky, V. Y. *Russ. J. Phys. Chem.* **2012**, *86*, 1199−1203.

(31) Peng, B.; Yao, Y.; Zhao, C.; Lercher, J. A. *Angew. Chem.* **2012**, *124*, 2114−2117.

(32) Snåre, M.; Kubicková, I.; Mäki-Arvela, P.; Chichova, D.; Eränen, K.; Murzin, D. Y. *Fuel* **2008**, *87*, 933−945.